The generation and propagation of internal waves in Nootka Sound.

Senior Thesis

31st May 2015

Catherine Young

University of Washington

School of Oceanography, Box 357940

Seattle, Washington 98195-7940

cy9g12@soton.ac.uk

Acknowledgments

I would like to thank the University of Washington and the School of Oceanography for funding this study. I would also like to thank the crew of the R/V Thompson, and the students and faculty who took part in the Senior Thesis Cruise for their patience and assistance with the continuous depth checks, UCTD deployment and subsequent data acquisition. I would like to especially thank Charles Eriksen for advising me throughout the study and providing invaluable guidance. I thank Arthur Nowell for his continual help and guidance. Finally I would like to acknowledge and thank Jemima Rama and Robert Daniels for their constant help and support during all stages of this study.

Abstract

The inlets of Nootka Sound, British Columbia provide a favourable area to study internal wave generation and propagation due to their varying bottom topography, the presence of sills and the occurrence of semi-diurnal tides. For this study, current velocity profiles were collected using a ship mounted Acoustic Doppler Current Profiler (ADCP), and were complemented with CTD profiles from an UnderwayCTD (UCTD).Three mechanisms of internal wave generation were proposed, with one likely source of generation being due to the release of trapped internal waves at the head of the inlet with changing tidal phase from flood to ebb. There was also evidence for the excitation of baroclinic flow in the inlet. The importance of internal waves stems from their ability to transfer energy more efficiently than surface waves. This aids deep water mixing, which originates from turbulence at the sill and extends into the basin.

Introduction

A fjord is a mid to high-latitude long, narrow inlet/estuary formed by the advance of glaciers through mountainous terrain (Farmer and Freeland 1983; Ross et al. 2014). Interactions between barotrophic (gravity-driven) and baroclinic (density-driven) forcing is typical of fjordic systems (Robins and Elliott 2009) . Generally, the inlets found on the Pacific coast side of Vancouver Island are shorter, shallower -with an average depth of 125m - and narrower than those of the mainland coast. They also have shallower sills (Pickard 1963).

The riverine runoff into the west coast inlets is considerably less than into the mainland inlets, and has a winter maximum in contrast to the mainland summer maximum (Pickard 1963). The freshwater inputs depicted in Figure (1) show that this area (Gold River) is characterised by a large runoff from October to June, with a primary peak in December and a secondary peak in May, with falling levels from July to September. The riverine discharge during the period April to July is found to be higher than expected from the direct effects of precipitation alone, and therefore this indicates a significant contribution from snow melt that is drained by this river. The shape and location of fjords, such as the Nootka Sound fjords, combined with significant freshwater influence (mainly from rivers), gives rise to a brackish surface layer and a stratified water column (Pickard 1961). Although this data comes from 1961, the general trend still applies to

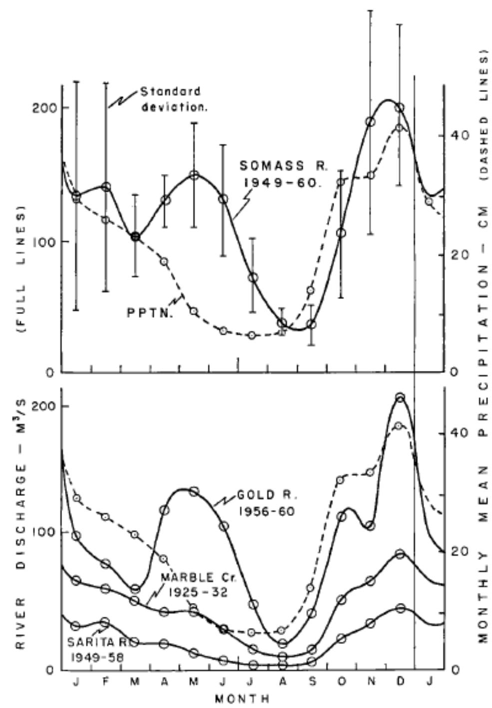

Figure 1 River discharge for four rivers flowing into inlets in Vancouver Island and monthly mean precipitation typical of Vancouver Island taken from Pickard (1963)

this area and has been noted by other authors including Drinkwater and Osborn (1975) when investigating tidal mixing in Rupert and Holberg Inlets, Vancouver Island.

Vlasenko et al. (2002) state that ‘the three important sources of motion in fjords, (i) freshwater runoff, (ii) tides, and (iii) the wind, interact and establish a complex circulation that occurs over a wide range of time and length scales.’ Farmer and Freeland (1983) suggest that wind stresses and internal waves/tides are the main mechanisms for mixing in fjords. Baroclinic tides are internal gravity waves of tidal frequency and are generated when barotrophic tidal currents encounter topographic slopes and displace density surfaces (Myrl and Garrett n.d.; Muller 2006). According to Morozov and Marchenko (2012), the interaction of the barotrophic tide and bottom topography is the most important source of internal wave generation, especially the presence of underwater sills, which are present in almost every fjord (Vlasenko et al. 2002; Ross et al. 2014).

On a large scale, sills and banks in the open ocean are amongst the principal generation sites of large non-linear internal waves, and are present in the ocean because of the existence of water column stratification (Vlasenko et al. 2005). Properties of internal waves differ from waves observed at the oceans’ surface; surface waves have an amplitude of at most a few meters, in comparison to internal wave amplitudes which can be as large as 100m or more in the open ocean (Muller 2006). They can thus create a hazard to offshore drilling operations with these waves remaining coherent for several days (Hyder et al. 2005; Jackson et al. 2012). In comparison to these large-scale open-ocean internal waves, an investigation by Pickard in 1961 found internal waves in Knight Inlet, British Columbia to be of a period of one to four minutes, with amplitude of up to 5m in the upper layers. At mid depths (20-150m), vertical oscillations of the isotherm with a semidiurnal period were common with amplitude of 5-75m. On both a large ocean scale and smaller scales, internal wave propagation represents an important energy transfer mechanism between tides and vertical mixing as it carries with it considerable velocity shear that leads to turbulence and mixing (Global Ocean Associates 2002). This often plays a key role in modification of the biological (primary production) environment (Sandstrom and Elliott 1984; Leichter et al. 1996). Internal waves influence the horizontal and vertical exchange processes in the ocean (Vlasenko et al. 2005) by affecting the transfer of heat, nutrients, and other properties within the water column (Huthnance 1995; Jackson et al. 2012) as well as the re-suspension of sediments and contaminant distributions.

According to Cummins et al. (2003) 'tidal flow over a sill appears to generate wave trains very close to the area of topographic interaction'. The sloping seabed imparts a vertical component to the stratified flow, displacing and therefore creating a depression in the pycnocline downstream of the sill. The flow gains a large phase speed relative to the moving water in order to remain stationary relative to the bank. The Froude number (Fr) is used to describe the flow pattern over an obstacle such as a sill.

$$Fr = \frac{v}{\sqrt{gh}} \qquad \textbf{(1)}$$

The Froude number is a dimensionless quantity that expresses the ratio of the average flow velocity (v) of a fluid to celerity, the speed of a shallow water wave ($c = \sqrt{gh}$ **).** If Fr<1 subcritical flow is inferred and the wave velocity is greater than flow velocity. As the flow slackens and turns subcritical (Fr<1), the lee wave can advance over the sill and propagate away from the generation zone. With sufficient energy, the waves steepen, break, and evolve into nonlinear internal waves (Jackson et al. 2012). In a two layered fluid flow over an obstacle, the important Froude number for internal wave generation is the internal Froude number, Fr_i.

$$Fr_i = Ri^{-\frac{1}{2}} = \frac{\Delta u}{\sqrt{-g\frac{\Delta\rho}{\rho_o}\Delta z}} \qquad \textbf{(2)}$$

Where g (equation 1) is replaced by reduced gravity$\left(g\,\frac{\Delta\rho}{\rho_o}\right)$, z is depth and u is the common approach velocity. A critical value of Fr_i corresponds to a fluid speed equal to the speed of long waves (Long n.d.).

Farmer and Dungan Smith (1980) observed an ‘upstream advance of a train of large amplitude lee waves with relaxation of the tidal current’ under conditions of water stratification similar to the conditions that are found in Nootka Sound. Restoration forces in internal waves are much smaller than restoring forces in surface waves. Smaller density differences (compared to the air/water interface) give way to waves with much longer periods, lengths and amplitudes than surface waves, as well as travelling at a slower speeds (Lafond 1962), and therefore internal wave propagation should be observed along the length of the inlets.

The increased understanding of internal wave generation and propagation has been achieved by in situ studies, the increasing availability of satellite imagery and from numerical models. Even with these advances in technology and understanding, no single mechanism has been found to fully describe the formation of internal waves over a sill. Many mechanisms and models have been proposed, such as the ‘lee wave mechanism’ (Maxworthy 1979). With such an important role in connecting large scale tides to smaller scale turbulence and mixing, internal waves will therefore remain an important study area.

The objective of this study is to propose possible mechanisms of internal wave formation and identify generation source of internal waves in Tahsis inlet, Nootka Sound, BC.

Methodology

Study area

Nootka Sound (49° 41' 11" N, 126° 33' 30" W) is located on the west coast of Vancouver Island and is made up of three inlets; Tahsis, Tlupana and Muchalat, connected by a common opening to the sea. Muchalat is the longest of the three inlets, and is fed by Gold River at the head. It has an inner (Williamson Sill) and outer sill at the mouth end, with depths of 70m and 55m respectively and an average mid inlet depth of 220m. Tahsis is the second longest of the three inlets and is fed by Tahsis River at its head and Tsowwin River (at Tsowwin Narrows), and is also connected to Esperanza inlet through the Tahsis Narrows. It is narrower and shallower than Muchalat, with an average mid inlet depth of 135m. The main Tahsis sill is located at Tsowwin Narrows and has a depth of 54m. The tidal influence over these sills is a potential source for internal wave formation.

2.2 Shipboard measurements

Measurements were collected between the 12th December and 20th December 2014 at various locations in Muchalat and Tahsis inlet. These surveys were conducted on the R/V Thomas G. Thompson.

In this study conductivity, temperature and pressure data was collected using two Oceanscience UnderwayCTD's (UCTD) (Teledyne Oceanscience 2014). Salinity was calculated from conductivity measurements, and density was calculated as a function of temperature, salinity and pressure. The main aim of using the UCTD was to gain an understanding of the temporal and spatial variation in salinity, temperature and density. The UCTD is a compact CTD which can be easily deployed and recovered from a moving vessel, allowing for multiple profiles to be taken in quick succession enabling high spatial resolution. The UCTD samples at a rate of 16Hz and has a drop speed of about 4m/s. When calculating the drop time, 20m was subtracted from the water depth and acted as a ‘buffer zone’ to prevent the UCTD colliding with the seafloor. The data collection included a 13 hour survey of Williamson sill, a 7 hour survey of Tsowwin Narrows sill, multiple along channel surveys in both inlets, and multiple stationary surveys in Tahsis. A total of 905 vertical profiles were taken during the study period. Stationary conductivity, temperature and pressure profiles were also collected using a SBE 911plus CTD.

Velocity was measured using the ship’s hull mounted 75kHz Acoustic Doppler Current Profiler (ADCP) for the whole duration of the study. The data was collected at 5 minute intervals from a depth of 35.47m downwards, at 8 meter bins.

The data is complimented by a bathymetric survey that took was conducted during the study period.

2. Post processing of data and numerical methods

Post processing in Matlab was used to parse, analyse and display the data. Each UCTD run consisted of up to 10 casts. The individual casts were defined based on vertical speed, pressure and conductivity by creating a minimum decent speed, minimum pressure and minimum conductivity that a section needed to fulfil to qualify as a cast (fig 1). As the UCTD is dropped vertically down the water column, the drop start time for each cast was referenced to the ships on board navigation system and therefore a location for each cast could be identified.

As the falling rate had some variability, measurements were taken at different depths and therefore records of temperature, salinity and pressure were evaluated by a least square fit model that was applied to the centre of a defined depth bin. UCTD conductivity offset and drift was corrected for by referencing the UCTD profiles to CTD profiles, assuming the temperature-salinity relation was the same for both instruments.

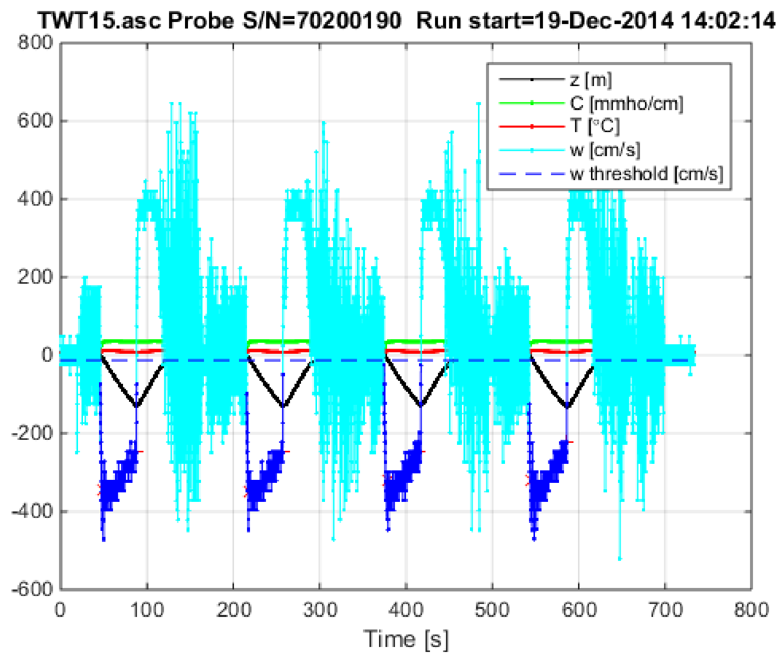

Figure 1 Identification of individual casts

Tahsis inlet was selected to be the focus of the study due to the greater data availability that spanned over the tidal cycle. Seven repeat transects that spanned from Tsowwin Narrows to Tahsis River were analysed.

Results

Average temperature, salinity and density anomaly ($\sigma_T = \rho(S,T) - 1000$, where $\rho(S,T)$ is surface density at the sea surface for temperature T and Salinity S), profiles were calculated for Tahsis inlet using multiple deep casts that were taken over the varying tidal cycle (fig 2). The maximum depths of theses casts were 147m, and therefore did not capture the whole water column, of which the maximum depth is around 200m.

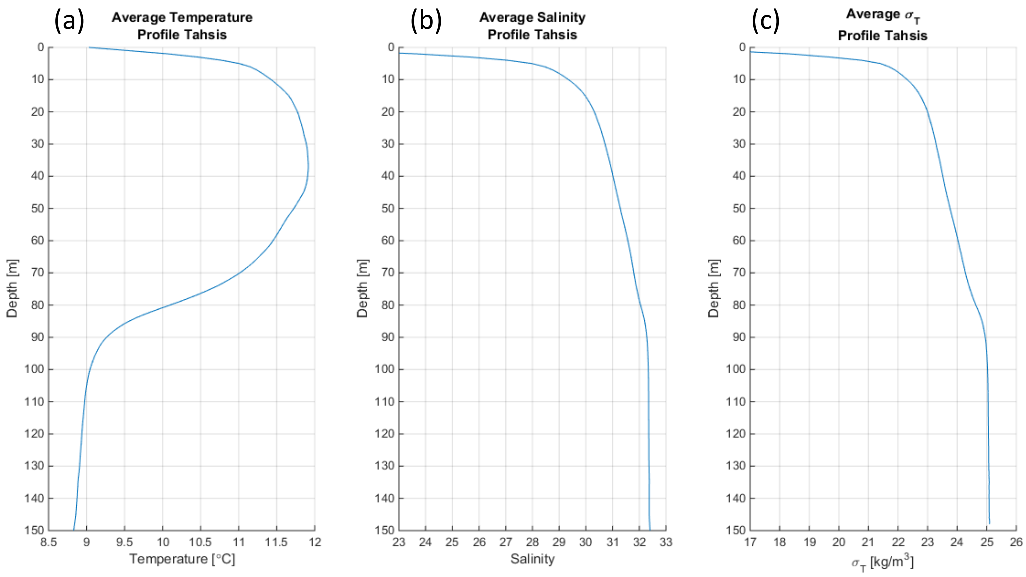

Figure 2 Mean (a) Temperature, (b) Salinity and (c) $\boldsymbol{\sigma_T}$ profiles for Tahsis inlet

As there is a temperature inversion (maxima at 40m depth) within the water column (fig 2(a)) density anomaly was used as the indicator for variation within the water column due to its monotonic function.

The sw_bfrq routine was executed in Matlab, using the average temperature and salinity profiles (fig 2), to produce a profile of the Brunt–Väisälä (buoyancy) frequency with depth ($N_{(Z)}$) (fig 3).

$$N_{(Z)} = \left(-\frac{g}{\rho_O}\frac{\partial \rho}{\partial z}\right)^{\frac{1}{2}} \qquad \textbf{(3)}$$

Where g is gravitational acceleration, $\rho_O$is a reference density, $\partial\rho/\partial z$ is the density distribution as a function of

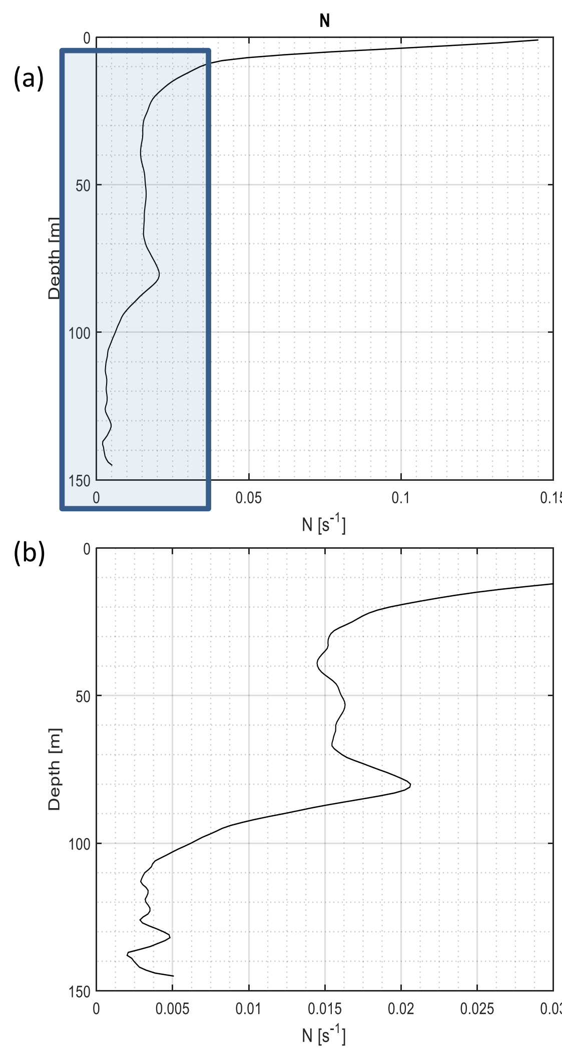

Figure 3 (a) Brunt–Väisälä frequency (N) with depth. (b) Shows an enlargement of the selected area in (a). Note change in axis scale.

depth, z. The buoyancy frequency characterises the water column stratification and is the frequency at which a vertically displaced parcel will oscillate within a statically stable environment. As all values N>0, the water column stratification is seen to be stable. The buoyancy frequency generally decreases with depth, with a slight increasing peak at a depth of around 80m. This peak coincides with both the thermocline depth (fig 2(a)) and the depth of the northward/southward velocity flow interface (0ms^{-1}) (fig 4(h-n)).

Temperature, σ_T profiles and density displacement profiles (fig 4) were calculated using the average σ_T profiles and were used as initial indicators for the possible presence of internal waves (fig 4).

Figure 4 (a-g) shows seven along channel sections in Tahsis inlet from the sill to the head. (a)-(c) cover the two flood stages of the 17th December tidal cycle. (a) represents the end of ebb to the very beginning of flood, and (b) and (c) represent the mid flood stage.(d)-(g) cover the ebb stage of the tidal cycle two days later, with (d) representing the beginning of the ebb, (e) and (f) spanning across the ebb, and (g) representing close to the end of the ebb. Variation in vertical displacement can clearly be seen in figure 4(f) and figure 4(g) at a distance of 8km and 7.5km from the sill respectively during ebb flow. At these locations, an upwards displacement of up to 8 m can be observed at a depth of 15-50m. This area of maximum displacement moves 500m in a southerly direction over a time period of 37 minutes: $c = 0.225\ ms^{-1}$.

The ADCP data shows a strong (upwards of 0.06ms^{-1}) northwards flow in the upper 75-80m during the initial flood stage of the tidal cycle in figure 4(a) over the sill, which coincides with a downwards displacement of the water closest to the sill. Below 80m, the flow is southwards and weaker (0.02 – 0.04 ms$^{-1)}$. Later on in the flood stage (fig 4(b), 4(c)), there is still a clear but weaker northward flow direction in the upper water column (0.03-0.05ms^{-1}), and the lower water column southward flow velocity is moderately reduced (0-0.02ms^{-1}). Vertical displacement along these profiles is relatively uniform with little/no downwards displacement.

Ebb flow shows a direct contrast to flood, with the upper water column (above 80m) moving in a southwards direction and the lower water column moving in a northwards direction. During the ebb stage of the tidal cycle (fig 4(d)-(f)), a strong southward velocity current can be seen in the upper 75-80m (0.06ms^{-1} upwards). Downwards displacement is clear to see in figure 4(e-g) around the sill (0 km) and up to 4km indicating the downwelling of water due to the constricted flow over the sill. Northwards current is present during ebb at depths below 85m, and is relatively strong around these areas of topographical interaction (0.04-0.08ms^{-1}).

Figure 4 (h-n) shows the mean velocity profile for each section, the overall mean velocity value for each section- which can be taken to represent the barotrophic flow, and the resultant baroclinic flow calculated with the removal of the barotrophic flow from the mean velocity profile. With the exception of figure 4(j), the flood and ebb generally appear to be mirror images of each other. At around 80 m in all profiles (fig 4 (h-n)), there is a rapid change of velocity from positive to negative or vice versa. This is the region of maximum shear between the northward and southward velocity flow layers. Figure 5 shows the first five vertical modes for the CTD Station T04.

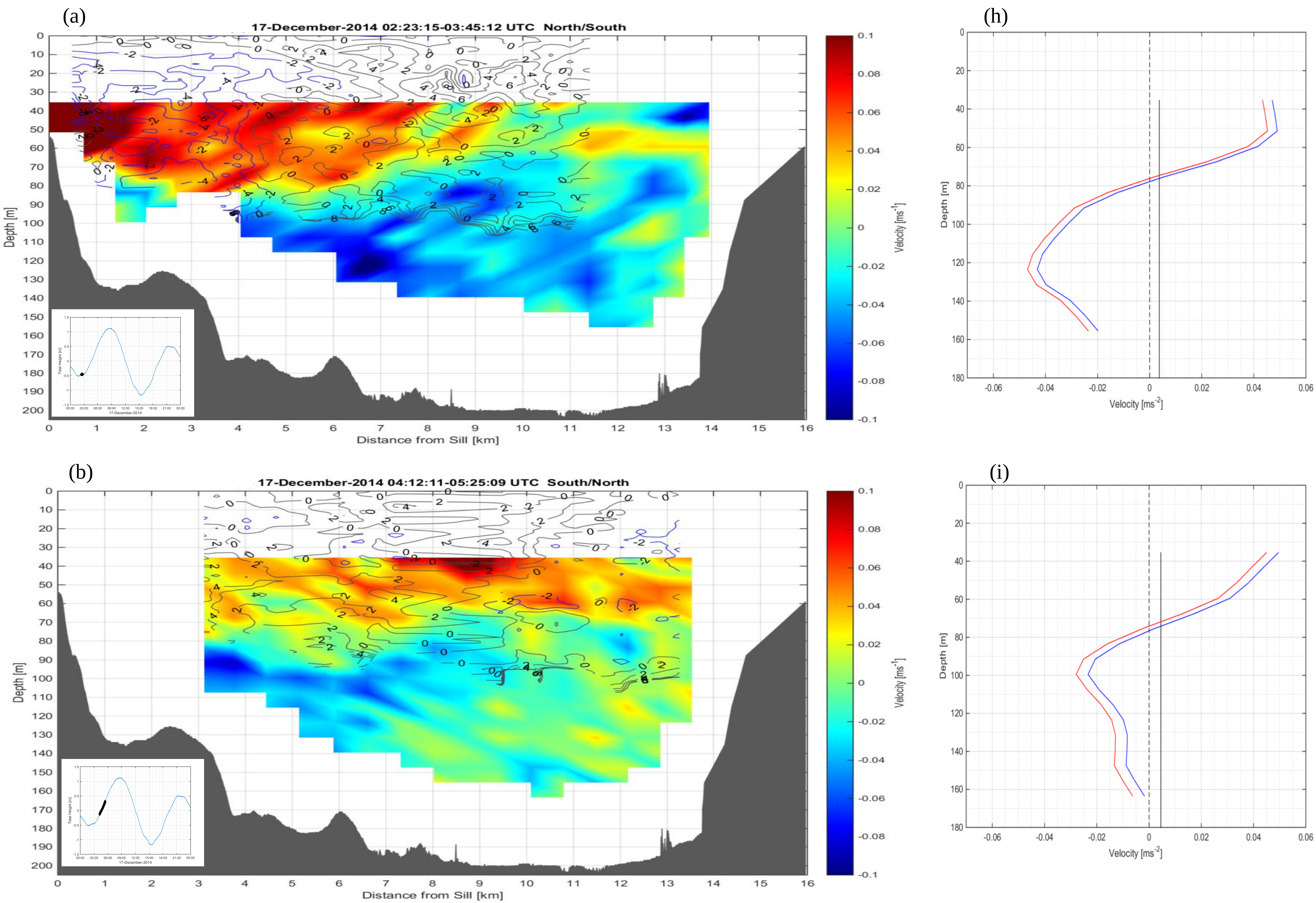
(a)
17-December-2014 02:23:15-03:45:12 UTC North/South
Depth [m]
Distance from Sill [km]
Velocity [ms-1]
(b)
17-December-2014 04:12:11-05:25:09 UTC South/North
Depth [m]
Distance from Sill [km]
Velocity [ms-1]
(h)
Depth [m]
Velocity [ms-2]
(i)
Depth [m]
Velocity [ms-2]

(c)

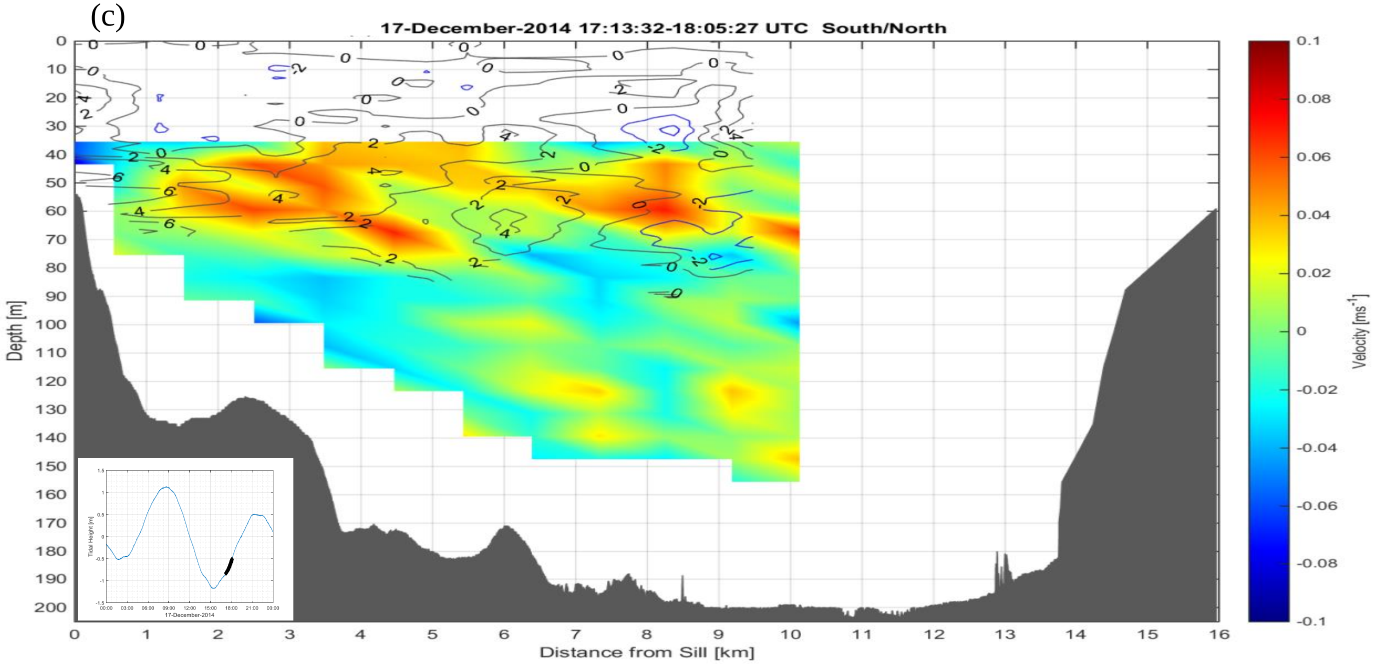

17-December-2014 17:13:32-18:05:27 UTC South/North
Depth [m]
Distance from Sill [km]
Velocity [ms-1]

(j)

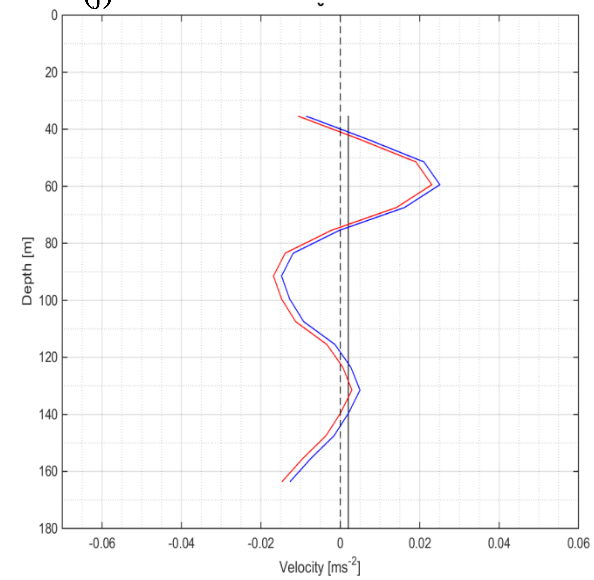

Depth [m]
Velocity [ms-2]

(d)

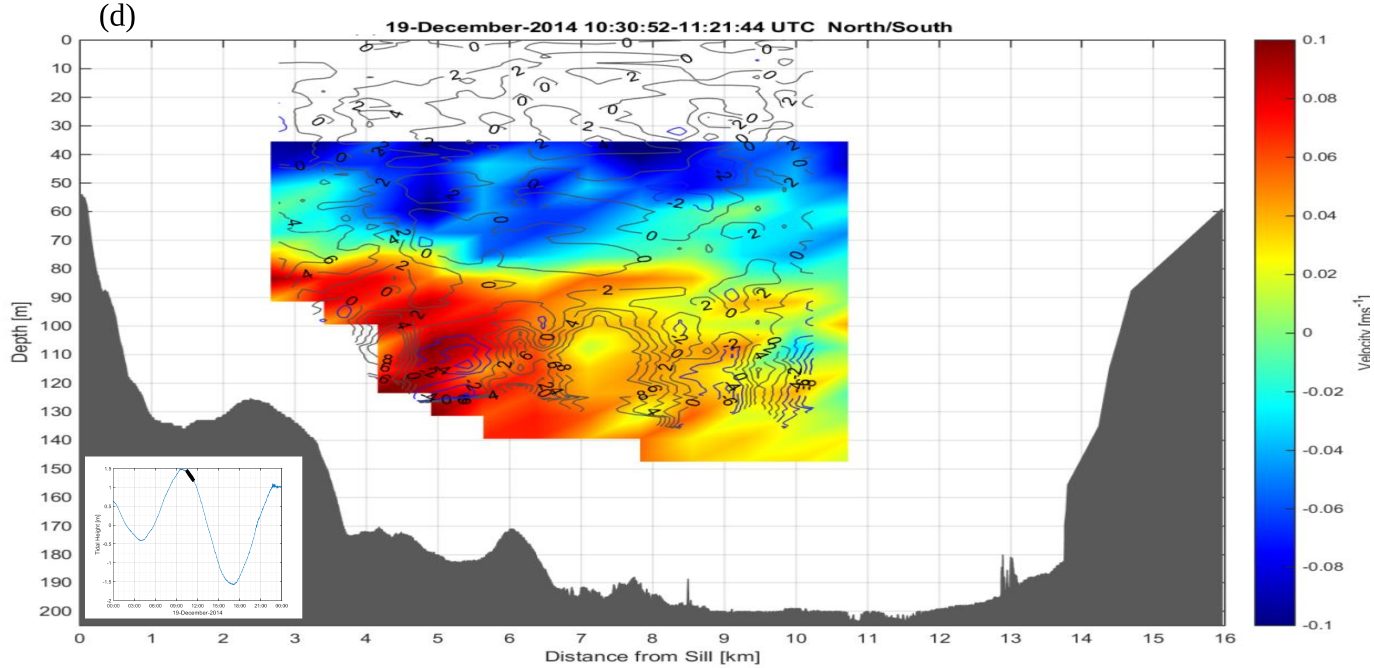

19-December-2014 10:30:52-11:21:44 UTC North/South
Depth [m]
Distance from Sill [km]
Velocity [ms-1]

(k)

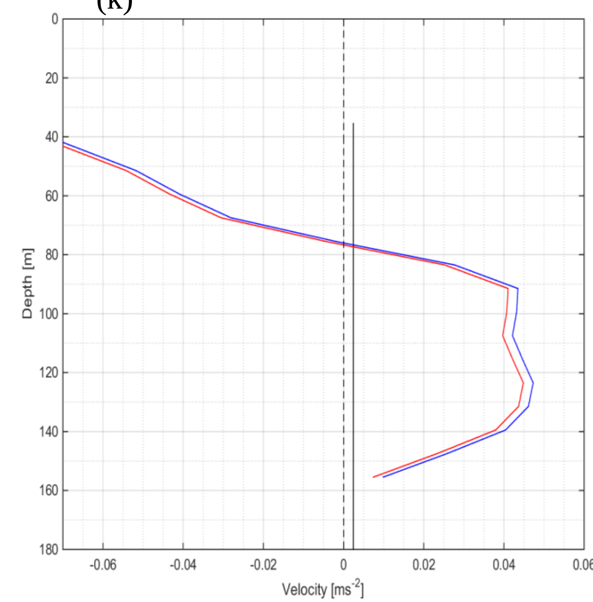

Depth [m]
Velocity [ms-2]

(e)

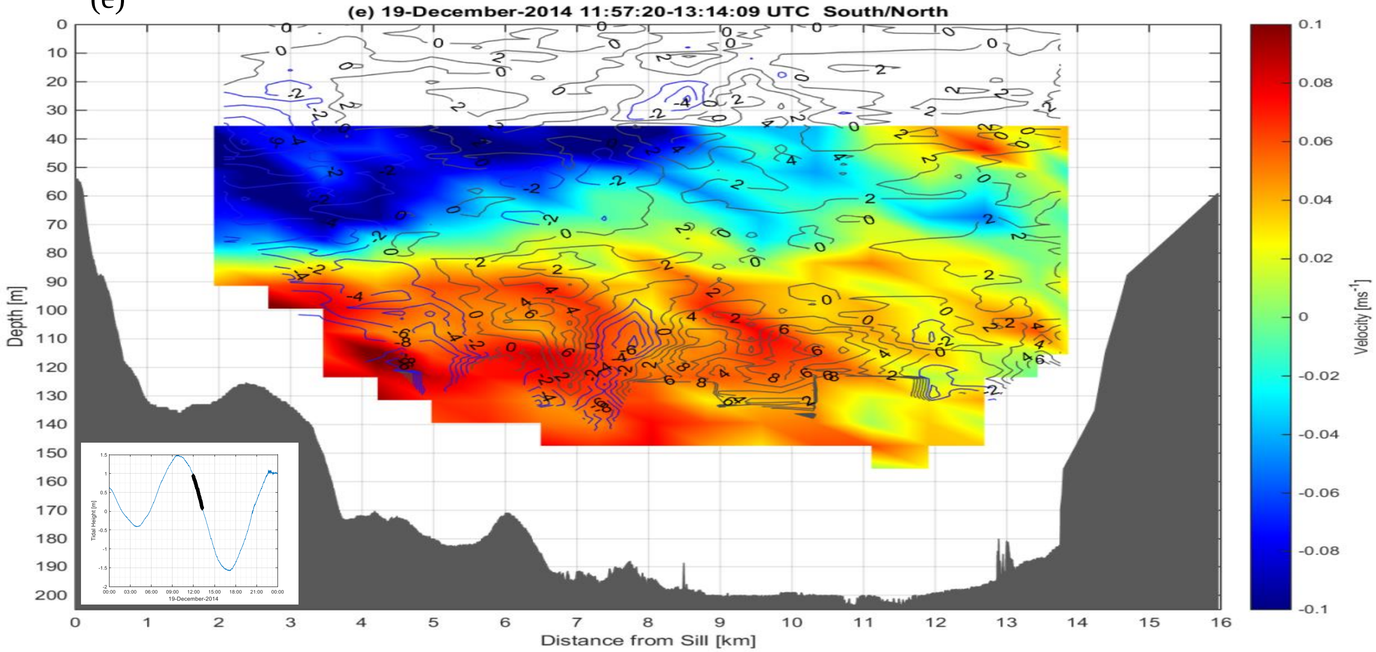
(e) 19-December-2014 11:57:20-13:14:09 UTC South/North
Depth [m]
Distance from Sill [km]
Velocity [ms^{-1}]

(l)

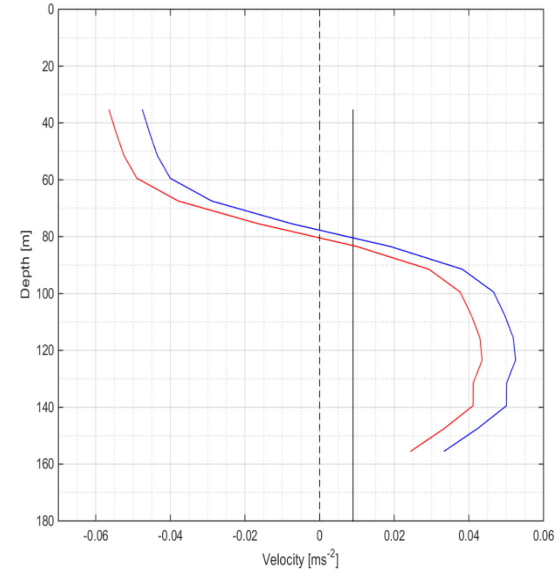
Depth [m]
Velocity [ms^{-2}]

(f)

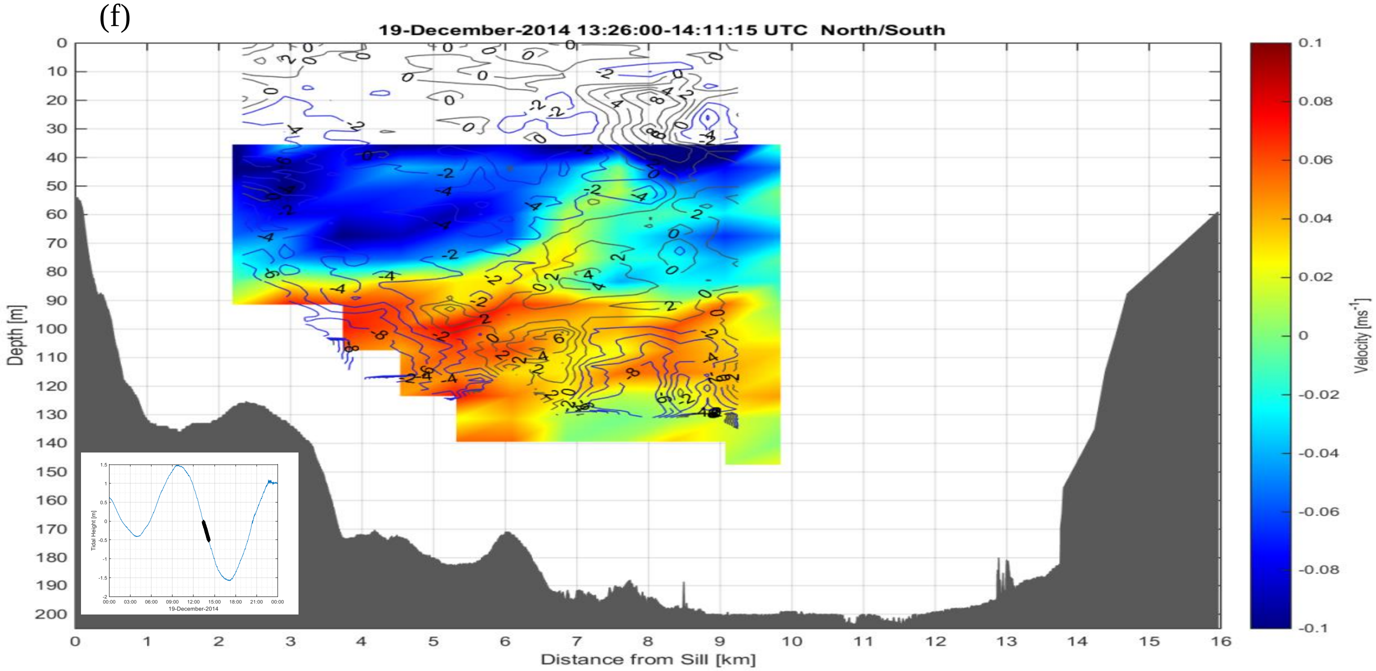
19-December-2014 13:26:00-14:11:15 UTC North/South
Depth [m]
Distance from Sill [km]
Velocity [ms^{-1}]

(m)

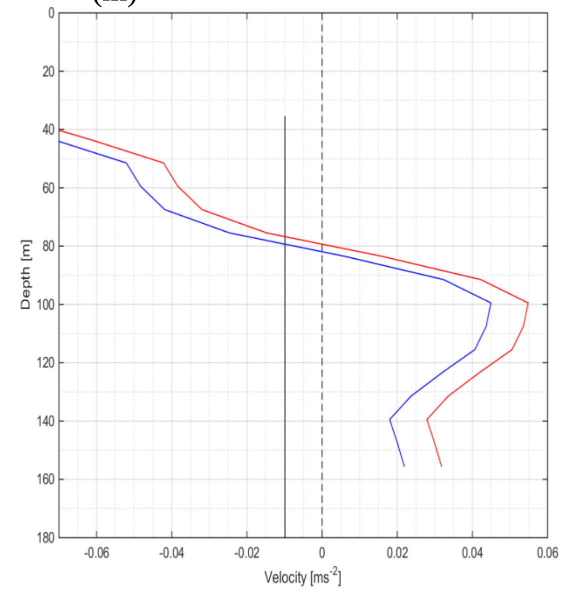
Depth [m]
Velocity [ms^{-2}]

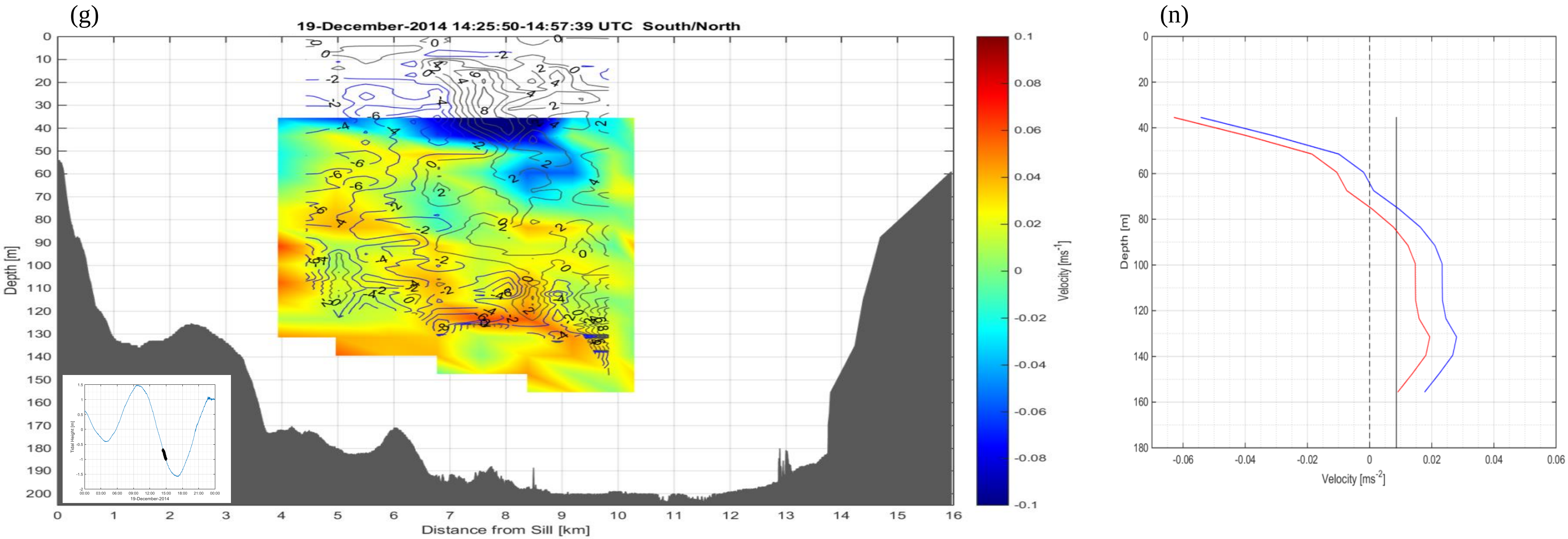

Figure 4

(a)-(g) Velocity [ms-1] (colour map with positive values indicating northward current) and vertical displacement [m] of density surfaces from the average σ_T profile (upwards displacement indicating by dark grey contour lines and downward displacement indicated by blue contour lines). Distance along channel is from Tsowwin Narrows Sill (at 0km) towards Tahsis River (North) [km]. Stage of the tidal cycle that the measurements were acquired during is shown by the black line. Tidal measurements are taken from Gore Island.

(h)-(n) Profiles correspond to adjacent channel sections. Mean velocity value for whole section ($< \bar{\boldsymbol{U}} >$) (barotrophic flow) (black line), mean velocity profile with depth for whole section ($< \boldsymbol{U} >$) (blue line), mean velocity profile - mean velocity value ($< \boldsymbol{U} > \; - < \bar{\boldsymbol{U}} >$) (baroclinic flow) (red line).

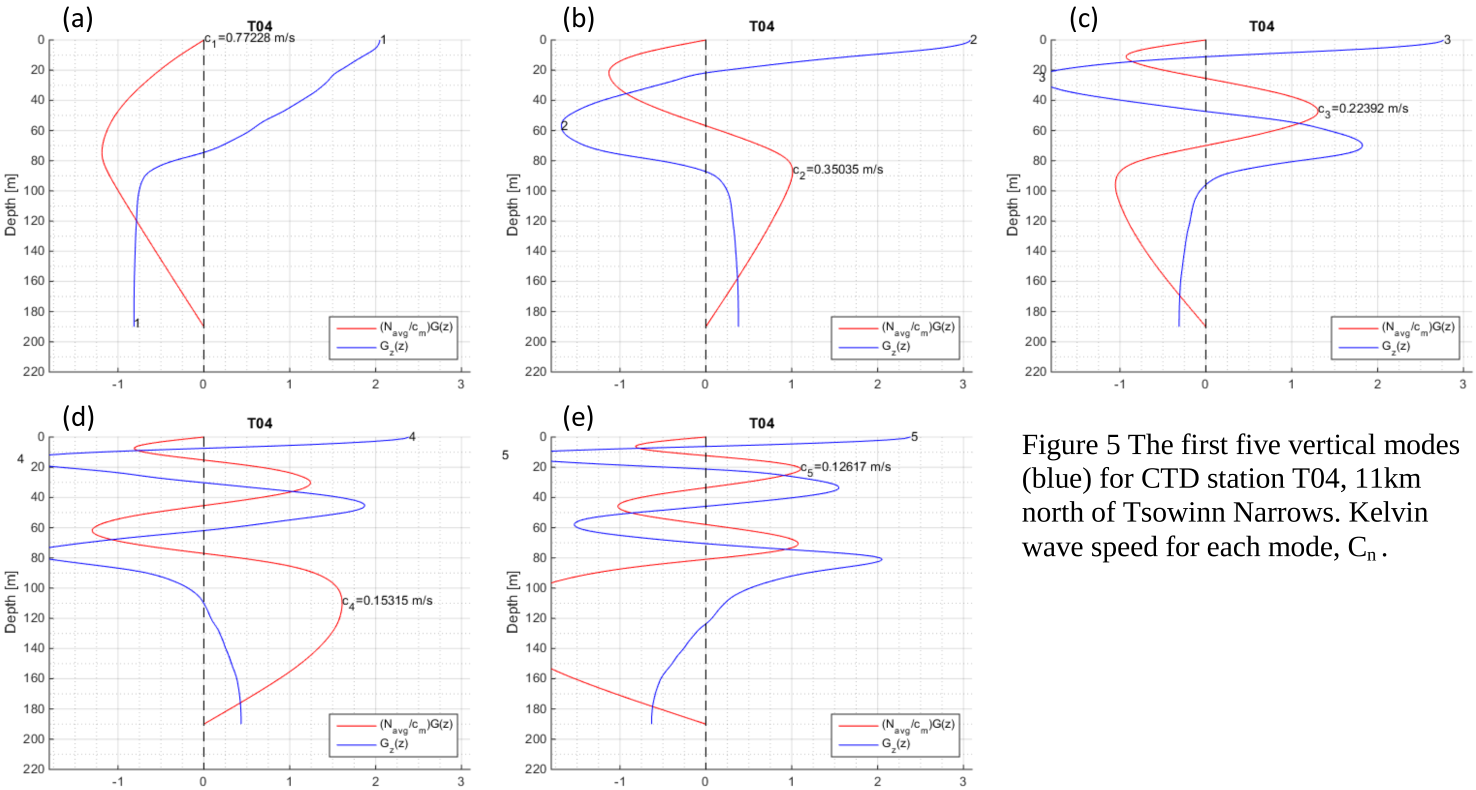

Figure 5 The first five vertical modes (blue) for CTD station T04, 11km north of Tsowinn Narrows. Kelvin wave speed for each mode, C_n .

Discussion

It must firstly be stated that the beam-like structures in the ADCP data are likely to be an artefact of the processing of the data, rather than velocity beam signals. This was identified as the slope of these beam-like structures changed significantly based on the direction of transit up or down the inlet. Therefore the hydrostatic internal wave dispersion relation and slope of the phase surface could not be calculated based on these profiles. Another limitation of the data is that the interaction of the velocity currents with the topography at the northern end of the inlet could not be analysed due to the lack of data in this area.

Wave generation

Ross et al. (2014) and Farmer and Freeland (1983), both suggest three internal wave generation mechanisms. 1) Generation over topography such as a sill. 2) Generation by tidal motion or internal currents over the sloping shore near the head of a fjord. 3) Generated at the beginning of ebb, when the flow changes from supercritical to subcritical. In this case, the internal waves are trapped until the internal wave phase speed surpasses the river plume velocity. The internal waves are then shed from the plume front.

During the flood tide, there is a strong flow (>0.1ms^{-1}) over the sill (fig 4(a)), which coincides with a large area of negative displacement that stretches from the sill for 4km, and an area of positive displacement that stretches from 6km from the sill to 10km from the sill. The change between the mid flood and beginning of ebb is clear to see with the upper water column in fig 4(d) moving in a southerly direction with velocities of (-) 0.02 to 0.1 ms^{-1}. Fig 4(e) shows an increase in the energy in the upper section of the inlet towards the head. As mentioned earlier, fig 4(f) and 4(g) show an area of high upwards displacement at 8km and 7.5 km from the sill with negative (strong southward) velocities associated with this area of positive displacement. Therefore the third theory mentioned above may be applicable to Tahsis inlet as a generation mechanism for internal waves.

Baroclinic modes

The M2 barotrophic tide dominates in this area. In figure 4 (h, I, k-m), the shape of the calculated baroclinic flow is very similar to the shape of the first baroclinic vertical mode (fig 5(a)). The shape of the calculated baroclinic flow in figure 4(j) possibly represents a higher baroclinic vertical mode (fig 5 (c-e)). Barotrophic tidal flow over steep topography such as a sill, forces the stratified water column up or down the slope, and results in a transfer of energy from the barotrophic tide into internal (baroclinic) waves (Simmons et al. 2004). The conversion of barotrophic to baroclinic flow occurs in regions where the topographic slope is critical or nearly critical with respect to the direction of the propagating internal tide (Holt and Thorpe 1997; Mattias Green et al. 2008). The downward displacement of density isopycnals the water column around the sill (fig 4(a, d-g)), and the strength of the calculated baroclinic tide in comparison to the calculated barotrophic tide (fig 4 (h-n)) therefore suggests an excitation of baroclinic flow and support the first theory mentioned above.

Conclusion

The use of a UCTD enabled a better temporal and spatial understanding of the temperature, salinity and density in the inlets in comparison to the deployment of a stationary CTD rosette. Further investigation into the generation of internal waves as the head of an inlet could prove an alternate mechanism for internal wave generation, which is rarely described in the literature, in comparison to internal wave generation over sills.

References

Cummins, P. F., Vagle, S., Armi, L., and Farmer, D. M. 2003. Stratified flow over topography: upstream influence and generation of nonlinear internal waves. Proc. R. Soc. A Math. Phys. Eng. Sci. **459**: 1467–1487.

Drinkwater, K. F., and Osborn, T. R. 1975. The role of tidal mixing in Rupert and Holbcrg Inlets, Vancouver Island. Limnol. Oceanogr. **20**: 518–529.

Farmer, D. M., and Dungan Smith, J. 1980. Tidal interaction of stratified flow with a sill in Knight Inlet. Deep Sea Res. Part A. Oceanogr. Res. Pap. **27**: 239–254.

Farmer, D. M., and Freeland, H. J. 1983. The Physical Oceanography of Fjords. Prog. Oceanogr. **12**: 147–220.

Global Ocean Associates. 2002. Oceanic Internal Waves and Solitons. An Atlas Ocean. Intern. Solitary Waves 1–40.

Holt, J. T., and Thorpe, S. a. 1997. The propagation of high frequency internal waves in the Celtic Sea. Deep Sea Res. Part I Oceanogr. Res. Pap. **44**: 2087–2116.

Huthnance, J. M. 1995. Circulation, exchange and water masses at the ocean margin: the role of physical processes at the shelf edge. Prog. Oceanogr. **35**: 353–431.

Hyder, P., Jeans, D. R. G., Cauquil, E., and Nerzic, R. 2005. Observations and predictability of internal solitons in the northern Andaman Sea. Appl. Ocean Res. **27**: 1–11.

Jackson, C. R., da Silva, J. C. B., and Jeans, G. 2012. The generation of nonlinear internal waves. Oceanography **25**: 108–123.

Lafond, E. C. 1962. Physical Oceanography Volume 1 Internal Waves, p. 731–751. *In* THE SEA Ideas and Observations on Progress in the Study of the Seas.

Leichter, J. J., Wing, S. R., Miller, S. L., and Denny, M. 1996. Pulsed delivery of subthermocline water to Conch Reef (Florida Keys) by internal tidal bores. Limnol. Oceanogr. **41**: 1490–1501.

Long, R. R. n.d. National Committee for Fluid Mechanics Films: Film Notes for Stratified Flow. Accessed on 30th May 2015 at http://web.mit.edu/hml/ncfmf/18SF.pdf

Mattias Green, J. a., Simpson, J. H., Legg, S., and Palmer, M. R. 2008. Internal waves, baroclinic energy fluxes and mixing at the European shelf edge. Cont. Shelf Res. **28**: 937–950.

Maxworthy, T. 1979. A note on the internal solitary waves produced by tidal flow over a three-dimensional ridge. J. Geophys. Res. **84**: 338–346.

Morozov, E. G., and Marchenko, A. V. 2012. Short-period internal waves in an arctic Fjord (Spitsbergen). Izv. Atmos. Ocean. Phys. **48**: 401–408.

Muller, P. 2006. Review of Baroclinic Tides: Theoretical Modeline and Observational Evidence by V. Vlasenko, N. Stashchuck, and K. Hutter. Oceanography **19**: 195–197.

Myrl, H., and Garrett, C. n.d. Lecture 6: Internal Tides. 77–99. Accessed on 15th May 2015 at https://www.whoi.edu/fileserver.do?id=21356&pt=10&p=17272

Pickard, G. L. 1961. Oceanographic Features of Inlets in the British Columbia Mainland Coast. J. Fish. Res. Board Canada **18**: 907–999.

Pickard, G. L. 1963. Oceanographic Characteristics of Inlets of Vancouver Island British Columbia. J. Fish. Res. Board Canada **20**: 1109–1144.

Robins, P. E., and Elliott, A. J. 2009. The internal tide of the Gareloch, a Scottish Fjord. Estuar. Coast. Shelf Sci. **81**: 130–142.

Ross, L., Pérez-Santos, I., Valle-Levinson, A., and Schneider, W. 2014. Semidiurnal internal tides in a Patagonian fjord. Prog. Oceanogr. **129**: 19–34.

Sandstrom, H., and Elliott, J. A. 1984. Internal tide and solitons on the Scotian Shelf: A nutrient pump at work. J. Geophys. Res. **89**: 6415.

Simmons, H. L., Hallberg, R. W., and Arbic, B. K. 2004. Internal wave generation in a global baroclinic tide model. Deep. Res. Part II Top. Stud. Oceanogr. **51**: 3043–3068.

TeledyneOceanscience. 2014. Accessed 12th May 2015 at http://www.oceanscience.com/products/underway-systems/underway-ctd.aspx.

Vlasenko, V., Stashchuk, N., and Hutter, K. 2002. Water exchange in fjords induced by tidally generated internal lee waves. Dyn. Atmos. Ocean. **35**: 63–89.

Vlasenko, V., Stashchuk, N., and Hutter, K. 2005. Baroclinic Tides: Theoretical Modeling and Observational Evidence, Cambridge University Press.